PCCP

The Evolution of Solvation Symmetry and Composition in Zn Halide Aqueous Solutions from Dilute to Extreme Concentrations

Journal:	*Physical Chemistry Chemical Physics*
Manuscript ID	CP-ART-04-2023-001559.R1
Article Type:	Paper
Date Submitted by the Author:	19-Jun-2023
Complete List of Authors:	Dhakal, Diwash; University of Washington Driscoll, Darren; Argonne National Laboratory Govind, Niranjan; Pacific Northwest National Laboratory Stack, Andrew; Oak Ridge National Laboratory Rampal, Nikhil; Oak Ridge National Laboratory Schenter, Gregory; Pacific Northwest National Laboratory Mundy, Christopher; Pacific Northwest National Laboratory Fister, Tim; Argonne National Laboratory Fulton, John; Pacific Northwest National Laboratory Balasubramanian, Mahalingam; Oak Ridge National Laboratory Seidler, Gerald; University of Washington

The Evolution of Solvation Symmetry and Composition in Zn Halide Aqueous Solutions from Dilute to Extreme Concentrations

Diwash Dhakal[1], Darren M. Driscoll[2], Niranjan Govind[4], Andrew G. Stack[3], Nikhil Rampal[3,5], Gregory Schenter[4], Christopher J. Mundy[4], Timothy T. Fister[7], John L. Fulton[4], Mahalingam Balasubramanian[2], Gerald T. Seidler[6,c]

[1] Materials Science and Engineering Department, University of Washington, Seattle, WA 98195, USA
[2] X-ray Sciences Division, Argonne National Laboratory, Lemont, IL 60439, USA
[3] Oak Ridge National Laboratory, TN, 37831, USA
[4] Physical Science Division, Pacific Northwest National Laboratory, Richland, WA 99352, USA
[5] Department of Chemical Engineering, Columbia University, New York, NY 10027, USA
[6] Physics Department, University of Washington, Seattle, WA 98195, USA
[7] Chemical Sciences and Engineering Division, Argonne National Laboratory, Lemont, IL 60439, USA

Abstract

The emergence of cation-anion species, or contact ion pairs, is fundamental to understanding the physical properties of aqueous solutions when moving from the ideal, low-concentration limit to the manifestly non-ideal limits of very high solute concentration or constituent ion activity. We focus here on Zn halide solutions both as a model system and also as an exemplar of the applications spanning from (i) electrical energy storage via the paradigm of water in salt electrolyte (WiSE) to (ii) the physical chemistry of brines in geochemistry to (iii) the long-standing problem of nucleation. Using a combination of experimental and theoretical approaches we quantify the halide coordination number and changing coordination geometry without embedded use of theoretical equilibrium constants. These results and the associated methods, notably including the use of valence-to-core x-ray emission spectroscopy, provide new insights into the Zn halide system and new research directions in the physical chemistry of concentrated electrolytes.

(c) corresponding author: seidler@uw.edu

I. Introduction

The structure and resulting chemical and electronic properties of aqueous solutions is central to the coupled experimental and theoretical development of physical chemistry. Specifically, any comprehensive understanding must address the classic progression from ideal dilute solutions with uncoordinated solute ions to, first, more concentrated cases requiring nontrivial activity coefficients and sophisticated thermodynamic modeling to, finally, more extreme cases with strong anion-cation coordination. (1-3) This sequence of conditions still bears contemporary relevance both as a testing ground of, e.g., *ab initio* molecular dynamics, and also for the accelerating importance of both traditional concentrated solutions and ionic liquids across numerous fields of research and technology. (4-7)

We report a combined experimental and theoretical investigation of ion pairing in Zn-halide aqueous solutions over their full accessible concentration range. This is, on one hand, undeniably a model system that is highly amenable to modern theoretical treatments and, on the other hand, is also deeply relevant for electrical energy storage, for geochemical processes, and for the fundamental understanding of the dynamics and influence of ion association on precipitation of solid phases. (8-15)

To begin, following the successful demonstration of rechargeable Zn-ion intercalation chemistry and the introduction of the highly concentrated electrolyte concept, there is growing interest in Zn-based multivalent aqueous chemistry (16-18) due to the higher energy density promised by a multivalent battery and the nontoxicity and earth-abundance of Zn. (19, 20) Significantly motivating the present work, recent studies (16, 21) of so-called ‘water-in-salt

electrolytes' (WiSE) for aqueous batteries have shown that the presence and extent of ion pairing in an aqueous electrolyte plays a vital role in enlarging the electrochemical window of the electrolyte, thus increasing stored energy density. This includes $ZnCl_2$ WiSE in Zn-ion batteries, which show enhanced performance at high salt concentrations, both in pure and mixed salt solutions. (12-15) The presence of ion-paired complexes, especially the tetrahedral $ZnCl_4^{2-}$ complex, at such high salt concentrations is believed to be essential to the improved performance. However, neither the extent of ion pairing nor its exact correlation with the resulting electrochemical properties are well understood.

In fact, the detailed occurrence of contact ion pairing in aqueous $ZnCl_2$ solutions remains uncertain despite extensive prior work for a completely different reason: the physical chemistry of geochemical brines. The solubilities of minerals are influenced by the type and concentration of ligands present in the brine. Metal complexes with different ligands contribute to the overall solubility in varying degrees and thus it is very important to understand the distribution of various complexes in an aqueous solution. (9) As chloride is considered to be the dominant anion in most natural hydrothermal solutions and furthermore as chloride complexes of Zn are considered the main species responsible for Zn transport in such systems, the evolution of ion pairing in aqueous $ZnCl_2$ is central to understanding the transport mechanisms for Zn in hydrothermal brines, (9, 22, 23) and its successful modeling can inform other geochemical processes.

Finally, the extent of ion association in complex aqueous solutions, particularly with respect to the mechanisms of precipitation of solid phases, is an even broader topic with strong and contentious contemporary interest. (10, 24-28) Linking the atomic-scale structure and dynamics of the solution to the elementary reaction mechanisms by which nucleation occurs is an inherently difficult problem due to the transient nature of nucleation reactions and intermediates

involved in their formation and the range of different types of potential solutes in solutions (see e.g., Wang et al., 2022 (29)). There is growing evidence that the longer-range solution structure, i.e., outside the immediate first solvation shell, can induce changes in the reactivity of ion complexes and subsequent phase selection and rates during nucleation reactions. (30, 31) This is especially true at high concentrations, where classical notions about the nature of activity-concentration relationships of solutes become invalidated. $ZnCl_2$ is a good test case for ideas about extended networks of associated ions because it is known to have ion complexes and has a high solubility that is facile for solution structure measurements. That being said, there remains broad disagreement about the nature of the speciation and the degree and distribution of higher order complex formation. (30) Given the uncertainties here, considerable benefit would accrue from a firm characterization of the Zn^{+2} first-shell coordination across the relevant range of concentrations, ion activity, and even temperature. Such a result would serve as a powerful anchor for theoretical treatment in the difficult, highly concentrated (and hence highly correlated) domain, and also would be strong prior information for improved interpretation of extended x-ray absorption fine structure (EXAFS).

Hence, in all cases the central questions surround the relative domains of thermodynamic stability or coexistence for the variety of local coordinations of the Zn^{+2} ion, as shown in Fig. 1 and Fig. SI-1 and tabulated in Table SI-1. For temperatures near ambient, several studies of Zn-Cl solutions agree that (1) there is predominantly octahedrally-coordinated $Zn(H_2O)_6^{2+}$ at low Zn concentrations and low anion activity, and that (2) there is predominantly tetrahedrally-coordinated $ZnCl_4^{2-}$ at very high anion activity.(8, 9) However, these works disagree on the intermediate regime, in some cases suggesting that other moieties, such as partially-hydrated and partially chlorinated Zn^{+2} in a tetrahedral environment, can be thermodynamically favored. To

this end, aqueous Zn-halide solutions have seen previous detailed study of the local and extended solvation structure by EXAFS (9, 11, 32), XANES (22), x-ray diffraction (33, 34) and neutron diffraction (35).

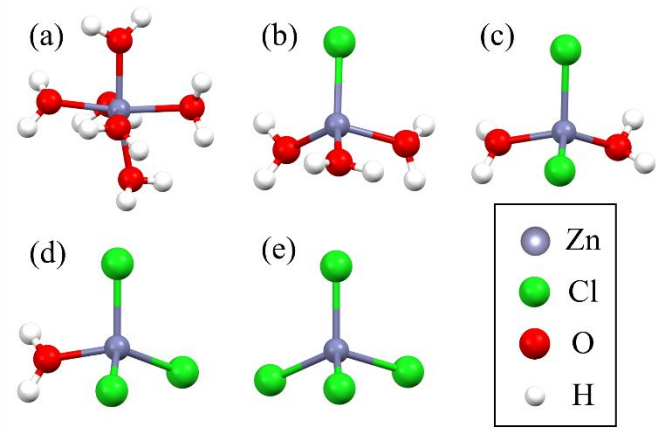

Figure 1. DFT-optimized Zn^{+2} coordination structures for (a) $Zn(H_2O)_6^{+2}$, (b) $ZnCl(H_2O)_3^{+}$, (c) $ZnCl_2(H_2O)_2$, (d) $ZnCl_3(H_2O)^{-}$, (e) $ZnCl_4^{-2}$. In all cases, hybrid DFT based optimizations using the PBE0 exchange-correlation functional was performed with 40 explicit water molecules, while the long-range solvation was treated implicitly. For clarity, the water molecules beyond the first shell are not shown.

In the present work on $ZnCl_2$ and $ZnBr_2$ aqueous solutions we employ two complementary experimental methods having direct sensitivity to the question of local coordination: XANES, where we extend prior work to higher concentrations, and valence-to-core x-ray emission spectroscopy (VTC-XES), being used here for the first time on this class of question. The VTC-XES results, which measure the occupied density of states near the Fermi level, show unambiguous, and quite significantly, an exclusive sensitivity to the first-shell coordination, unlike XANES, which is also sensitive to the overall environment up to higher shells. This distinction is

due to the locality of occupied states in this system as opposed to the delocalization of unoccupied states – recall that Zn^{2+} has no unoccupied 3*d* derived states, so there are no localized pre-edge features in the XANES.

With support from time-dependent density functional theory (TDDFT), we find that the VTC-XES allows inference of the number of chloride ligands per Zn ion, henceforth N_{Cl}. The resulting proposed dependence of N_{Cl} on Zn salt concentration or on total Cl concentration when other salts are added is compared and contrasted with Classical Molecular Dynamics (CMD) and lattice Monte Carlo (MC) calculations. Our study provides a new benchmark for ion pairing in Zn halide systems while also presenting a new methodology for studying first-shell coordination in concentrated solutions.

II. Methods

II.A. Materials and Solutions

For both the XES and XANES studies, aqueous solution samples of $Zn(NO_3)_2$, $ZnCl_2$, and $ZnBr_2$, often with added chloride salts (LiCl or NaCl) or bromide salts (LiBr), were prepared in air by dissolving weighed amounts of respective salts in HPLC-grade water. For higher concentrations, a magnetic stirrer was used for ~30 minutes to generate clear samples without visual sign of undissolved solute. Aqueous solution samples of ZnO and $Zn(OH)_2$ with added KOH were similarly prepared in air. The anhydrous $ZnCl_2$ polycrystalline reference sample was prepared in a glovebox starting with anhydrous $ZnCl_2$. ZnO and $Zn(OH)_2$ polycrystalline samples were prepared in air. All reagents were purchased from standard vendors (Alfa-Aesar, Sigma Aldrich, Fisher Scientific) in 99.9% purity or higher. For XES experiments, the solution samples were then

loaded into thin-walled quartz capillaries (Charles Supper Corp.) closed with sealing wax. A significant air space was included in the capillary to accommodate possible evolved gas during x-ray irradiation. For XAS experiments, solutions were placed within PEEK holders of varying thickness having polyimide windows and sealed with epoxy.

II.B. X-ray Emission Spectroscopy (XES)

The XES measurements were performed with a laboratory-based x-ray emission spectrometer, described in detail in Jahrman, et al. (36) The x-ray source has a Pd anode and was operated at ~100 W power (35 kV and 2.8 mA). A Ge (555) spherically bent crystal analyzer had favorable Bragg angles and energy resolution for the required energy range. The vertical capillary sample holders were placed ~5 mm away from the Be exit window of the x-ray tube. Optimal lateral placement with respect to the vertical entrance slit of the spectrometer was verified by the method of Mortensen, et al. (37)

Each Zn XES scan spanned both the main Kβ line and the valence-to-core (VTC) region. Specifically, the scans were collected over the energy range 9550 – 9700 eV in 0.25-eV steps. We use a 40 s integration time per point in a region spanning the VTC emission (9630 – 9680 eV) and a shorter 4 s integration time per point in a lower-energy region spanning the main Kβ peak (9550 – 9630 eV) and a higher-energy region (9680 – 9700 eV) taken to assist with background subtraction. Total measurement times for each solution sample were typically 24 h for the Cl-containing solutions and 36 h for the Br-containing solutions. Comparison of early and later scans shows no evidence of beam damage. The average sample temperature was ~42°C for Cl-containing solutions and ~25°C for Br-containing solutions. The higher temperature of the Cl-containing

solutions was due to heating from the end of the x-ray tube and was avoided for the Br-containing studies by adding a fan blowing on the sample location. A few representative Cl-containing solutions, especially in the intermediate concentration range where the temperature dependence is expected to be the strongest and hence serve as the upper bound of the mismatch, were also measured at 25°C. As shown in Fig. SI-2 there is only a small systematic difference between the spectra measured at the two temperatures, resulting in <5% change in the inferred octahedral contribution (discussed in detail below and in the results and discussion).

Frequent measurement of the Kβ emission for a metallic Zn reference served as a check against any monochromator drift and allowed correction for instrumental calibration across multiple experiments, often separated by other uses of the spectrometer. The final energy scale is consistent across all data sets to ~25 meV.

Processing of the XES data followed several steps. First, we subtracted a constant background with value typically <5% of the count rate in the VTC region; this was due to stray scatter of the primary x-ray radiation. We found the relative Zn Kβ line shape and energy within our measurements to be invariant across metallic Zn and all solutions studied, due to the filled $3d^{10}$ shells for Zn^{+2}. A common shift in Bragg angle was thus applied to all the spectra to align our measurements with the accepted absolute energy value of 9572 eV for the Kβ line in literature. (38)See Fig. SI-3.

The invariance of the Zn Kβ spectra allows a unique approach to processing the VTC-XES results, wherein the spectra were brought to a consistent molar scale via integral normalization of the VTC-XES by the area under the Zn Kβ spectral feature (specifically from 9550 – 9600 eV). The success of this normalization is prerequisite for any inference of the relative population of different local coordinations of the Zn^{+2} ion. The dominant error in cross-

sample normalization of the VTC-XES will be from differences in the energy dependence of penetration of excitation radiation and escape of fluorescence at the main Kβ compared to the VTC region, and we estimate this contributes less than 3% error to the relative normalization of the valence-level emission with respect to the Kβ.

Enabled by the spectral normalization to a common mole-Zn scaled basis, a linear combination analysis of the various solution concentration series was used to infer information about the average number of chloride (or bromide) ligands per Zn ion. These fits were performed in Python using the VTC-XES data between 9640 – 9660 eV. The analysis utilized two solution end-point standards: a dilute ZnX_2 (X = Br^- or Cl^-) solution and a 1 m ZnX_2 solution with a very high concentration of added LiX salt to achieve the highest accessible anion activity.

II.C. X-ray Absorption Near Edge Structure (XANES)

X-ray absorption spectroscopy was performed at beamline 20-BM of the Advanced Photon Source. Aqueous solutions of $ZnCl_2$, $ZnBr_2$, LiCl, and LiBr of varying concentrations were placed in PEEK cells with polyimide windows and sealed with epoxy. XAS measurements were acquired in transmission mode by placing gas ionization chambers before (50% He, 50 % N_2) and after (100% N_2) each sample. The incident beam was reduced to a spot size of 1 mm horizontal by 0.5 mm vertical by a toroidal mirror. Harmonic rejection was performed using a Rh-coated flat mirror and detuning the incident beam by 15%. Spectra were acquired at the Zn K-edge and all spectra were energy aligned to that of the first derivate peak of a Zn reference foil (9660.76 eV).(39) Spectral background removal and normalization of the XAS spectra were performed within the Athena software program.(40)

The fact of background (per-atom or molar) normalization to the theoretical atomic background, in analogy with the discussion of normalization of the VTC-XES above, enables the attempt of a linear combination analysis of the different solution concentration series. The fits were performed in Athena using the XANES data between 9655 – 9675 eV. This analysis utilized two Zn K-edge solution standards: a dilute ZnX_2 ($X = Br^-$ or Cl^-) solution and a highly concentrated 5 m LiX solution with 0.25 m ZnX_2.

II.D. Density Functional Theory (DFT) & Time-Dependent Density Functional Theory (TDDFT) Calculations

All ground-state (DFT) and excited-state (TDDFT) calculations were performed with the NWChem quantum chemistry program.(41, 42). DFT-based optimizations of the Zn^{+2} coordination structures ($Zn(H_2O)_6^{+2}$, $ZnCl(H_2O)_3^+$, $ZnCl_2(H_2O)_2$, $ZnCl_3(H_2O)^-$, and $ZnCl_4^{-2}$) were performed with Zn represented with the Stuttgart relativistic small core (RSC) effective core potential (ECP) (43) and basis set, Cl represented with the Stuttgart relativistic large core (RLC) ECP (44) and basis and O and H atoms were represented with 6-31G* basis set.(45) All basis sets and ECPs were accessed from the EMSL Basis Set Exchange. (45) The exchange-correlation was treated with the global hybrid PBE0 functional. (46) In all cases a $ZnCl_x$ cluster with 40 waters was optimized while the long-range solvation was treated with implicit solvation (COSMO). (47) The resulting first-shell structures are shown in Fig. 1. Similar process was followed for the Zn-Br system, the resulting first-shell structures are shown in Fig. SI-1.

XANES and VTC-XES calculations were performed at the Zn K-edge for all optimized solvated $ZnCl_x$ clusters for comparison with the experimental spectra shown in Fig. 2. These

calculations were performed at the TDDFT level of theory. The XANES were computed with the TDDFT-based restricted excitation window approach, (48) which involves defining a model subspace of single excitations from the relevant core orbitals to the unoccupied orbitals. The VTC-XES were computed using the TDDFT-based protocol described in Reference (49). For these calculations, the Zn atom in all the clusters was represented with the Sapporo-TZP-2012 all-electron basis set(50) while the remaining atoms were represented as in the ground-state calculations. To describe excitations beyond the dipole approximation, higher-order contributions were included in the calculation of the oscillator strengths.

For comparison with experiment, all calculated XANES spectra were Lorentzian-broadened by 0.6 eV and shifted with a single common energy offset (+205 eV) across all spectra to align with the prominent XANES feature at 9670 eV for the $Zn(H_2O)_6^{+2}$ complex. Similarly, for comparison with experiment the TDDFT VTC-XES results were broadened by 1.5 eV and shifted with a single, common energy offset of 14.5 eV such that the tetrahedral spectral features aligned with the corresponding features on experimental spectra. The spectral intensities of the calculated VTC-XES were normalized using the area under the calculated main Kβ peak, the same process that was used for the experimental spectra (see section II.B. above).

II.E. Classical Molecular Dynamics Simulations and Models of Speciation

Classical Molecular Dynamics (CMD) simulations were performed using the LAMMPS (51) software package in the canonical (NVT) ensemble and the isothermal-isobaric (NPT) ensemble on a system containing zinc and/or lithium and chloride ions with SPC/E water. (52) The forcefield for $ZnCl_2$ was taken from previous work. (30) For LiCl, two sets of forcefields were

utilized. (53, 54) Interactions in the solution were represented by combining the Lennard-Jones potential and Coulombic interactions shifted to zero at 12 Å, where the cross-terms were defined using the Lorentz-Berthelot mixing rules (if they aren't explicitly defined in the forcefield). The particle-particle particle-mesh technique (55) was applied for long-range electrostatic force calculations.

Briefly, the initial configurations were generated using Packmol (56) with a tolerance of 2 Å. The equilibration of the system involved several steps. To begin, the system was equilibrated at 300 K in NVT ensemble for 2 ns, then to enhance the sampling, the temperature was ramped up to 1500 K and run for a further 5 ns. After the system was cooled down back to 300 K, the system was equilibrated in NPT ensemble for 5 ns. Finally, the trajectories were harvested during a 50 ns run in NVT ensemble.

To extend the results of the CMD simulations to a range of concentrations, the speciation was estimated using the geochemical speciation software PHREEQC, version 2.15. (57) The equilibrium constants for the formation of $ZnCl^{+}$, $ZnCl_2$, $ZnCl_3^{-}$, and $ZnCl_4^{-2}$ from aqueous Zn^{+2} and Cl^{-} were defined from the atomistic level simulation and the equilibrium concentration of each species calculated via mass balance and mass actions equations. For speciation in sodium chloride, aqueous Na^{+} was added to the species considered but without interaction with zinc or zinc chloride species. No other species were considered (i.e., the default databases were not used, but a custom model chemistry was created to reflect only the reactions as defined in Rampal et al., 2021 (30)). The average chloride per zinc was calculated by summing the concentrations of each individual chloride-bearing species, multiplied by the number of chlorines in the species, and divided by the total zinc concentration in the solution.

Several assumptions were tested to determine the sensitivity of the results. First, two different assumptions about activities were used, in the first, the activities for each species were estimated from the Davies equation, where at low ionic strengths it resembles the Debye-Hückel activity-concentration relationship but at high ionic strengths ($\gtrsim$ 1 molal) the activity coefficients start to increase by a factor twice the ionic strength. (58, 59) Alternately, no difference between activity and concentration was considered. The different ways to treat the activities changed the speciation differently at high and low ionic strengths, but did not substantively affect the maximum number of chlorines per zinc atom predicted. Additional tests included using equilibrium constants measured in 4.5 m versus 0.01 m solutions. Here, the equilibrium constants measured at 4.5 m predicted a more rapid rise in the number of chorines per zinc with concentration than those measured in 0.01 m solution, but both sets converged on the same number of chlorines per zinc at high concentrations.

Lastly, the role of dimer formation was considered. These were found previously to represent 5% of the ionic clusters in solution at 4.5 m $ZnCl_2$, comprised dominantly of $Zn_2Cl_5^-$ and Zn_2Cl_4 moieties (each contain a bridging chloride separating the two zincs). (30) Adding these species to speciation lowered the estimate of the maximum average number of chlorines per zinc by ~10%, or 0.2 chlorines per zinc for pure $ZnCl_2$. Based on the sum total of sensitivity analysis, the predicted speciation from the CMD simulations is thought to be fairly robust using this method.

II.F. Monte Carlo Simulations

In an effort to efficiently treat the collective correlation of ions with increasing concentration, a coarse-grained lattice Monte Carlo (MC) model was constructed that used

intermolecular potentials derived from the CMD simulations. At high concentrations (e.g. > 4.5 m) the increasingly glass-like behavior of most electrolyte solutions results in equilibrium timescales that are well beyond the reach of classical molecular dynamics. For this reason, MC is one of the few methods that can be used to realistically model the speciation at these extreme concentrations. For the CMD approach, the equilibrium constants derived from the MD trajectory at 4.5 m $ZnCl_2$ were used to predict speciation at extreme concentrations. The appropriateness of this assumption is unknown. Thus, MC potentially provides a significant improvement by directly calculating speciation at extreme concentrations using realistic representations of all ion-ion interactions that are increasingly important at short range.

The potential of mean force between all ion pairs in water were generated from an ensemble average using CMD simulations. From this, the long-range Coulomb interaction of the form $q_i q_j/\epsilon r_{ij}$ was removed to extract the short-range interaction of pairs, $u_{s,i,j}(r_{i,j})$, where the dielectric constant ϵ = 80 and q_a is the ionic charge. The influence of the water was approximated by its mean-field response to the ions. A periodic cubic lattice with lattice spacing 2 Å and with 20 lattice points in each Cartesian direction was constructed as the foundation of an approximate Monte Carlo scheme. We populate the lattice with an initial concentration of ions, n_a, a = Zn or Cl, randomly distributed with the full system charge neutral. Unoccupied sites represent a water background. Ions are constrained to be on lattice sites. The energy of the system, $U = \sum_{i<j}(u_{s,i,j}(r_{i,j}) + q_i q_j/\epsilon r_{ij})$ where interaction between periodic images is taken into account using an Ewald technique. (60, 61)

Metropolis Monte Carlo relaxation of the system was performed at an effective temperature of 300 K. Two types of moves were considered: ion-ion pair swaps and ion-vacancy swaps. The system was propagated until fluctuations in energy reached a constant mean value. Configurations

beyond this point were used as representative configurations of the ensemble to be used for evaluating averages. Fig. SI-4 depicts the short-range potential and the location of lattice interaction distances. From an ensemble of configurations, we were then able to calculate the connectivity and population of coordinated ions, i.e., the relative occurrence of the different hydrated and/or chlorinated moieties.

III. Results and Discussion

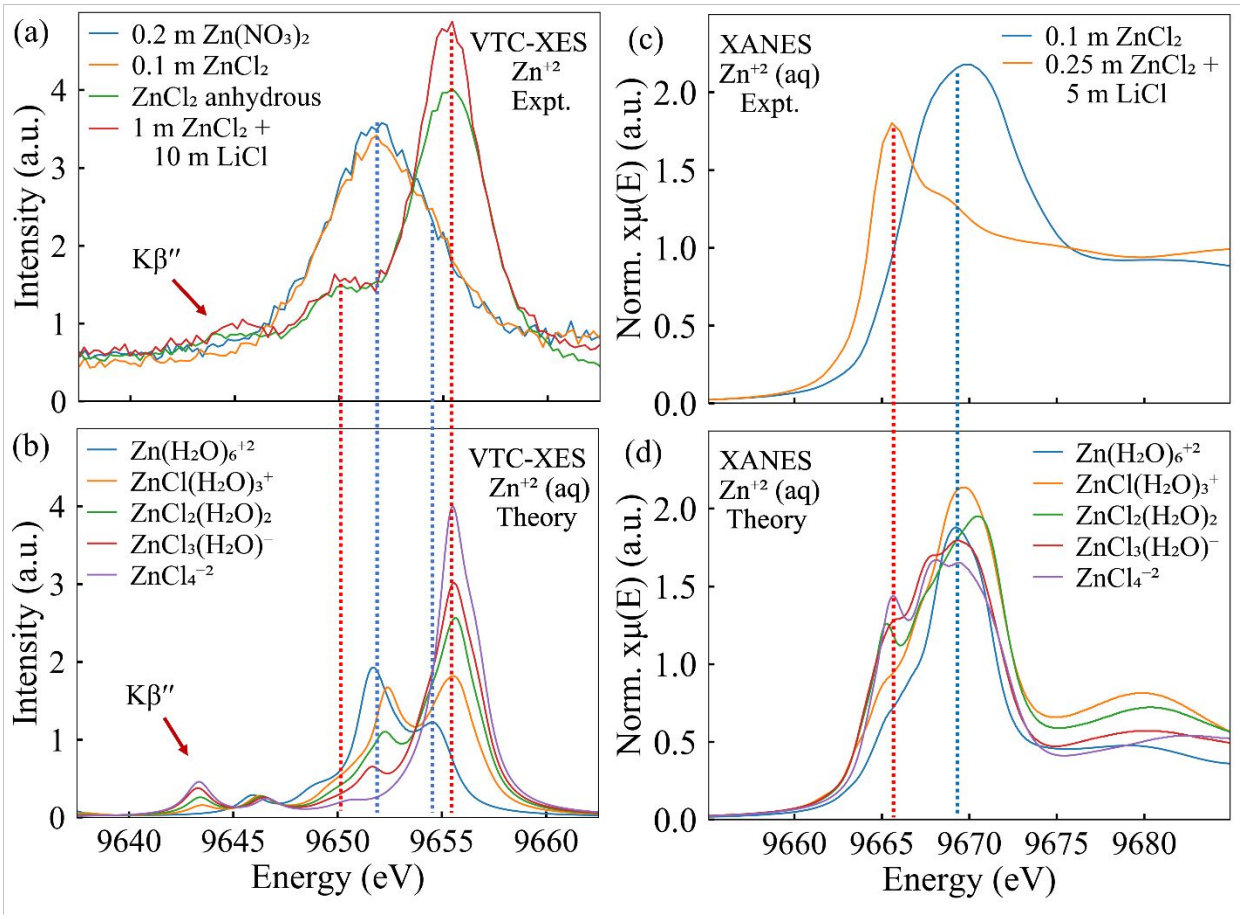

Figure 2. Comparison of VTC-XES (a) and (b) and XANES (c) and (d) between TDDFT theory and experimental results. The peak around 9645 eV in the VTC-XES spectra labeled as Kβ" in (a) and (b) is attributed to the transitions from Cl 3*s*-derived states to the Zn 1s orbital.

To begin, in Figure 2 we present the experimental and theoretical spectra for the endpoint species at the lowest and highest ion activities of this study. For both the VTC-XES and XANES spectra, the change from fully octahedrally coordinated $Zn(H_2O)_6^{+2}$ to nominally tetrahedrally coordinated $ZnCl_4^{-2}$ is apparent. For instance, similar spectral features in the XANES for $ZnCl_2$ solutions were reported in Liu et al., (22) and again similar features were observed in studies of other metal-halide systems. (62-64) For VTC-XES, unique spectral features assigned to either octahedral or tetrahedral symmetries in crystalline solids have been previously reported for Ti-based crystalline compounds by Gallo et al. (65) We have further confirmed these distinct spectral assignments for a series of Zn standards with supplementary measurements of ZnO, $Zn(OH)_2$, 0.5 m ZnO + 6 m KOH solution and 0.1 m $Zn(OH)_2$ + 6 m KOH solution, all of which have tetrahedral coordination of the Zn^{+2} ion and all of which show the same features, see Fig. SI-5. Again, the extreme locality of VTC-XES is particularly well-suited to the problem of first shell coordination and composition.

On the other hand, XANES theory only qualitatively matches the experimental spectra in that it does predict the emergence of the sharp feature at 9666 eV, but it fails to correctly predict the chemical evolution of the peak at 9669 eV. The VTC-XES predictions are stronger, with better matching of peaks and intensities and correct identification of the Cl ligand peak (Kβ'' in the figures). The theoretical spectra in Fig. 2 include not just the endpoint spectra, but also predictions for tetrahedral moieties with intermediate composition, e.g., that contain both some water and

some chlorine. Note that the progression from $Zn(H_2O)_6^{+2}$ to $ZnCl_4^{-2}$ is quite smooth as a function of the number of Cl ions in the tetrahedral moiety for VTC-XES but is more bimodal for XANES. This detail will play an important role in later discussion.

Next, in Figures 3 and 4 we present the experimental concentration series for the $ZnCl_2$ and $ZnBr_2$ systems, respectively. The spectral evolution follows Fig. 2, with the added point that achieving apparently complete conversion to $ZnCl_4^{-2}$ requires very high anion activity, here by added chlorine salts, i.e., the 1:2 composition ratio of Zn to Cl in the pure solutions is not apparently abetted by widespread polymerization.

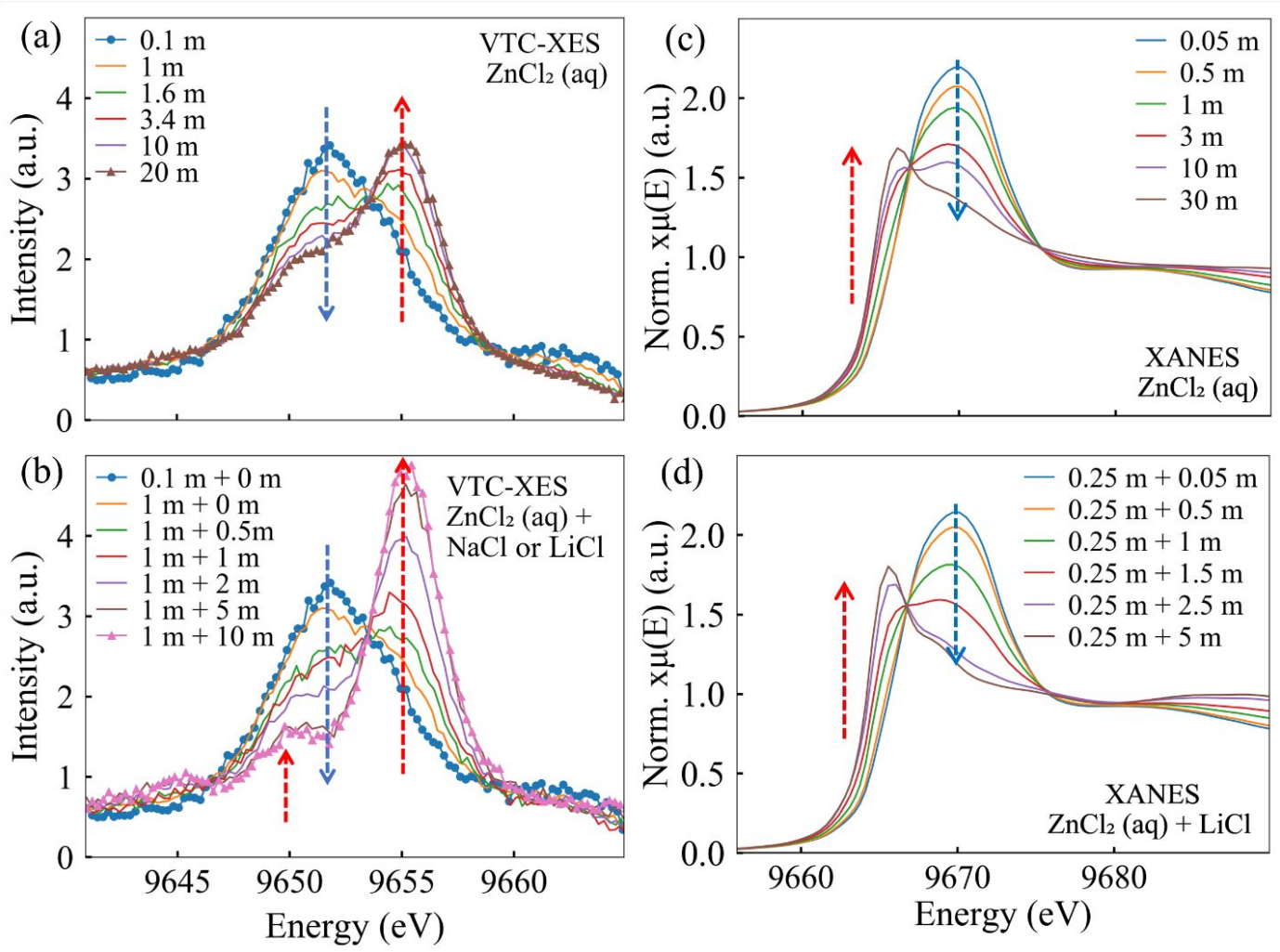

Figure 3. (a) and (c): VTC-XES and Zn K-edge XANES measurements of $ZnCl_2$ aqueous solution ranging from the dilute to the super-concentrated regime; (b) VTC-XES for 1 m $ZnCl_2$ with added

Cl salt; (d) Zn K-edge XANES for 0.25 m $ZnCl_2$ solution with added Cl salt. The blue and red arrows annotate peaks that correspond to octahedral and tetrahedral coordinations, respectively.

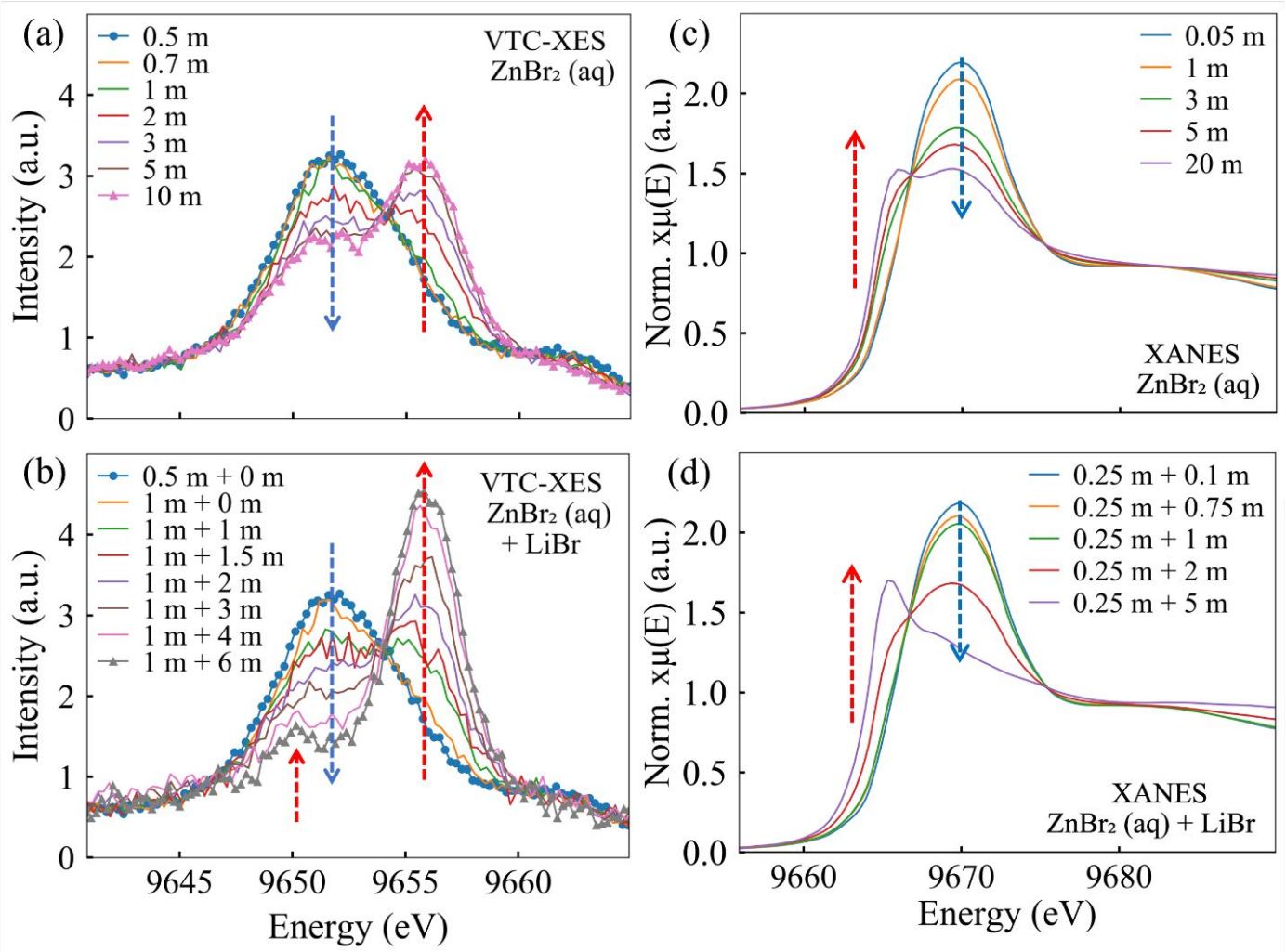

Figure 4. (a) and (c): VTC-XES and Zn K-edge XANES measurements of $ZnBr_2$ aqueous solution ranging from the dilute to the super-concentrated regime; (b) VTC-XES for 1 m $ZnBr_2$ with added

Br salt; (d) Zn K-edge XANES for 0.25 m $ZnBr_2$ solution with added Br salt. The blue and red arrows annotate peaks that correspond to octahedral and tetrahedral coordinations, respectively.

An added detail in Figures 3 and 4 merits discussion. Recall that all $\mu(E)$ are on a common mole basis because of standard normalization by the atomic background, and that all VTC-XES are also on a common mole basis because of our normalization via the integral of the Kβ diagram line intensity (see methods and Fig. SI-3), an approach that is justified by the filled $3d^{10}$ electronic configuration of the Zn^{+2} ion. Consequently, the existence of isosbestic (or, at least, quasi-isosbestic) points in all panels of both figures is suggestive, but not conclusive, of a simple mixture of the two endpoint moieties. This observation opens our inquiry into what details of the local Zn^{+2} coordination can be inferred from our results, and especially from the progression of results as a function of anion activity. In this, we progress through systematically more complex models for the Zn ion local environment, moving from a two-component model of only octahedral $Zn(H_2O)_6^{+2}$ and tetrahedral $ZnCl_4^{-2}$, to a model that allows for an intermediate series of partially hydrated tetrahedral moieties, and finally to the question of possible polymerization.

Hence, in Fig. 5, we show the result of decomposing the measured spectra for pure $ZnCl_2$ and pure $ZnBr_2$ solutions into a simple linear combination of the endpoint octahedral and fully chlorinated/brominated tetrahedral extremes. The relatively rapid onset of significant tetrahedral coordination with this conversion significantly saturating at ~3 – 5 m is obvious. The quality of these one-parameter fits are excellent for the VTC-XES (Fig. SI-6 – Fig. SI-9) which, again, is almost exclusively sensitive to the first coordination shell. By contrast, the fits are rather poor for the XANES spectra at high concentrations (Fig. SI-10), where contributions from higher solvation shell should be expected to break the basis of the local two-component model. That being said, it

is important to note that the measured octahedral fraction even for the VTC-XES appears to be at least slightly less than 0.5 (though within the estimated errors) at the highest concentration for both pure solution studies. This result is unintuitive because it corresponds to an average Zn-Cl coordination to be larger than two. It is worth noting that this equal segregation into octahedral Zn with six waters and tetrahedral Zn with four chlorides has been found to exist in crystals having a 3:2:1 composition ratio between water, chloride, and zinc. (66)

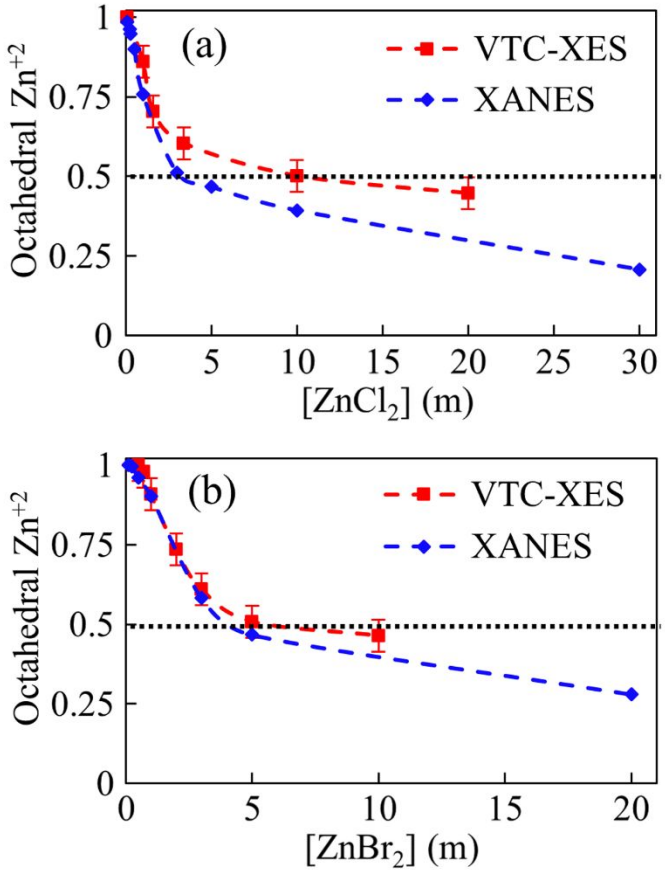

Figure 5. Linear combination analysis of XANES measurements and XES measurements for the $ZnCl_2$ (a) and $ZnBr_2$ (b) concentration series, based on a simple two-endpoint model. The vertical axis shows the *nominal* fraction of octahedral Zn^{+2} if there are no intermediate tetrahedral coordinations and if second-shell effects can be ignored.

While the occurrence of nominally isosbestic points in the mole-normalized spectra of Figures 3 and 4 suggests a simple two-component model, this is problematic. In fact, from a thermodynamic standpoint, several prior studies (9, 22, 32, 67) of $ZnCl_2$ solutions as a function of anion activity instead conclude that there must be some rich admixture of intermediate tetrahedral moieties of the form $Zn(H_2O)_{4-x}Cl_x^{2-x}$.

This brings us to the closely linked questions of (1) how to address the likely occurrence of intermediate moieties in our interpretation of spectra and (2) the reason for the surprisingly good VTC-XES fits for the one-parameter, two-component model, as per above and Fig. SI-6 – Fig. SI-9. Referring back to Fig. 2, note the TDDFT predicted VTC-XES for the range of likely Zn^{+2} environments is quite smooth in the Cl coordination number, *x*. Furthermore, because of a near-degeneracy of the octahedral fingerprint and one of the peaks in the tetrahedral spectra, the spectra for intermediate moieties are not very linearly independent from the endpoint spectra. While this scenario prohibits determination of the relative concentrations of chlorinated moieties, it does allow inference of the average number of chloride ligand (N_{Cl}) coordinated per Zn^{+2} ion via peak fitting performed on the calculated VTC-XES spectra (Table SI-3) and the one parameter fit results, see section 19 in the SI for a detailed treatment of this problem.

We present the inferred N_{Cl} for both the pure solution study and the high Cl concentration study in Fig. 6. The results for both systems are impressively physical: the pure solution study saturates at $N_{Cl} \approx 2$, the maximum value consistent with an absence of polymerization subject to the scale set when the high Cl concentration study reaches *the assumed value* $N_{Cl} = 4$, i.e., we have assumed the endpoint, highest-Cl-concentration sample itself is dominated by $ZnCl_4^{-2}$. We are comfortable with this assumption (i) because of the spectral similarities between the endpoint spectrum and the crystalline references, (ii) because of agreement with prior EXAFS study of

D'Angelo et al. (32) and (iii) because of the intuitive consistency of the result $N_{Cl} \approx 2$ for the pure solution case. Very similar results occur for $ZnBr_2$, see Fig. SI-11.

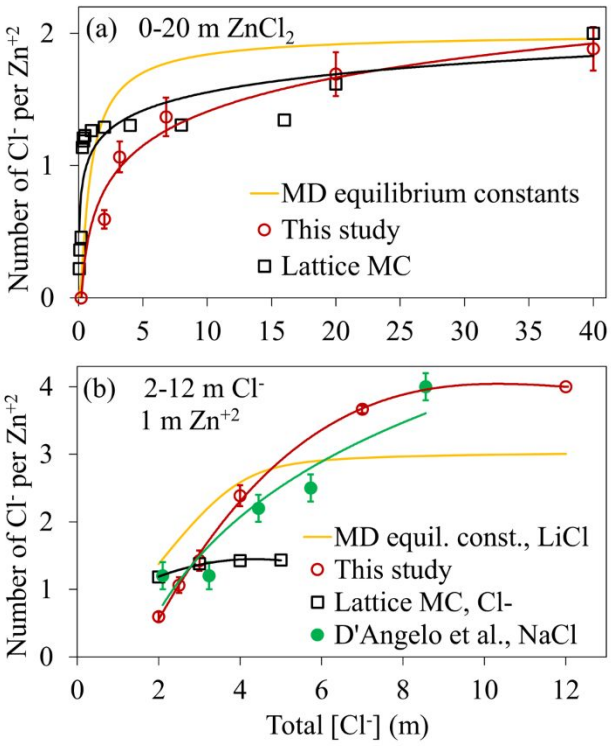

Fig. 6: Average number of Cl coordinated with Zn in the solution as a function of the total Cl concentration for (a) pure $ZnCl_2$ concentration series and (b) added salt series. The data from D'Angelo et al. (32) used molarity scale with 1 M $ZnCl_2$ and added NaCl and hence have slightly different Zn^{+2} concentrations between data points in the molal scale in this figure. The lines in the figure serve only as guides to the eye, except for the one labeled as "MD equilibrium constants".

However, it is important to recognize that these results differ from inferences in some prior work, both experiment and theory, and therefore there is considerable value in seeking additional perspectives on the Zn coordination, especially in the limit of high anion activity. For example, D'Angelo et al. (32) agree with $N_{Cl} = 4$ at high Cl ion activity, where this result is based entirely

on EXAFS data to infer coordination number, i.e., the conclusion drawn is purely from a structural point of view. On the other hand, Ruaya and Seward (23) disagree, finding a smaller estimate for N_{Cl} from an indirect analysis inferring of Zn complexes from the solubility of another salt (AgCl) and where the conclusion drawn is contingent on thermodynamic parameters.

This brings us to the classical molecular dynamics (CMD) simulations that we have performed on the same chemical systems. Qualitatively, a key, significant similarity between the CMD results and experiment is the observation of a relatively fast onset of substantial ion pairing with a tendency to saturation at intermediate concentrations. For a quantitative comparison of the CMD and experiment, in Fig. 6 we have included the curves for the average number of Cl^- ligands that were derived from the equilibrium constants generated from the CMD 1D Potential of Mean Force (PMF) calculations. The agreement for pure solutions is impressive: although theory predicts an even faster onset of ion pairing, there is complete agreement about the occurrence of saturation with two Cl^- neighbors and an absence of any significant polymerization.

However, in Fig. 6b, the agreement between the CMD and experimental results for the number of Cl^- is more problematic for the case with fixed Zn^{+2} concentration and high Cl^- activity, exactly where additional certainty about our experimentally motivated postulate that $N_{Cl} = 4$ would be most valuable. The CMD results do see, again, a quite strong drive toward ion pairing, but it almost entirely excludes the occurrence of $ZnCl_4^{-2}$. For more detail, in Fig. 7 we show the predicted relative populations of different Zn^{+2} moieties as a function of $ZnCl_2$ concentration (Fig. 7a) and as a function of total Cl^- concentration starting with 1 m $ZnCl_2$ and then adding supplemental Cl^- salts (Fig. 7b).

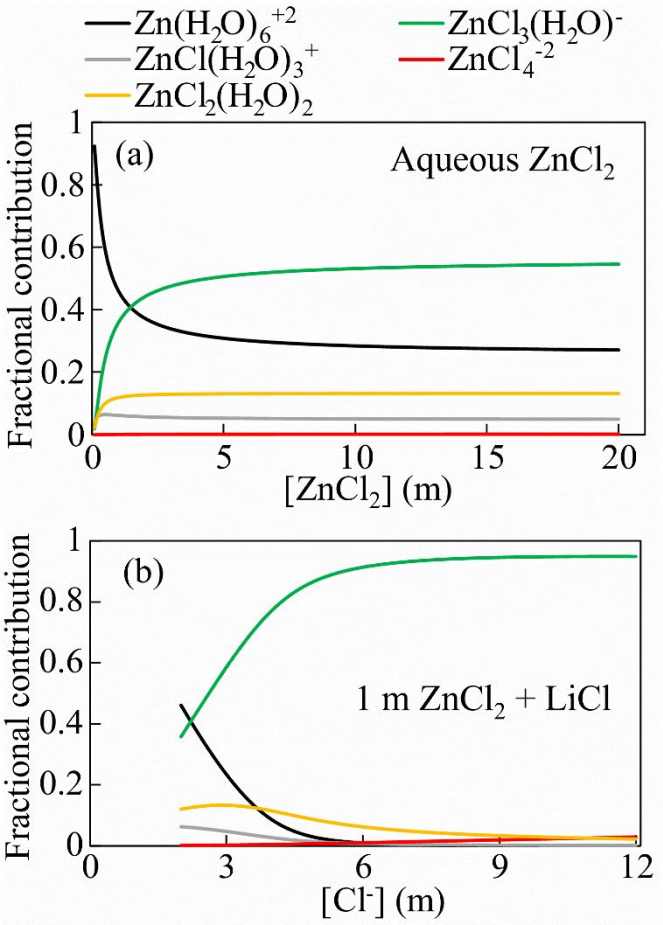

Figure. 7: Concentration dependent evolution of the concentrations of different moieties in pure $ZnCl_2$ solution (a) and 1 m $ZnCl_2$ + LiCl (b), calculated using CMD-derived equilibrium constants and assuming activities equal concentrations.

There are several potential sources for the discrepancy. First, it could be that the speciation predicted from CMD derived equilibrium constants are being extrapolated to conditions beyond their validity. As one test of this possibility, we ran explicit simulations of 1 m $ZnCl_2$ at multiple concentrations of LiCl using existing force fields for lithium. (53, 54) These simulations, the

results of which are included in the supporting information (Fig. SI-13), are consistent with the results of the predicted speciation from the CMD in Figure 6, with a maximum of three chlorides per zinc atom and consistent with speciation in prior CMD simulations (see Table SI-2 for a list). This rules out any issues with the speciation calculations, or the specific parameterization of the CMD force field. Second, there could be a systematic error in the speciation predicted by CMD. At this time however, we do not have a specific basis to understand the origin of this error, except to speculate that the extent of ion pairing is often overestimated in both formal charge and electronic continuum correction models. (29, 68) It is not difficult to envision that these types of errors could also result in a difficulty predicting correct stability of the zinc chloride tetramer. Third, there could be unforeseen issues with the interpretation of the experiments leading to an overestimation of the average number of chlorides surrounding the zinc. To get insight into this we compare the TDDFT calculated VTC-XES spectra of monomer $ZnCl_3^-$ complex with that of dimer $Zn_2Cl_5^-$ complex with one shared Cl. (Fig. SI-14) It should be noted that in both cases considered there are 3 Cl-ions coordinated with each Zn-ion. Our due diligence here was to confirm that the VTC-XES spectra are not sufficiently sensitive to presence of dimers.

Lastly, and perhaps most tantalizingly, there could be an unforeseen effect of lithium and/or sodium that influences the speciation of zinc chloride monomers that stabilizes zinc tetrachloride. Such effects have been observed in complex, highly concentrated solutions before, especially in their roles in solution dynamics and nucleation mechanisms (31) as well as aggregation phenomena (69) in alkaline aluminate solutions. This would not necessarily be predicted using the explicit simulations of the mixed solutions described in the supporting information (Fig. SI-13) since these are relying on mixing terms to provide the interaction between the sodium or lithium and the zinc

chloride species. However, we find no difference between the experimental VTC-XES spectra recorded for 1 m $ZnCl_2$ + 5 m LiCl and 1 m $ZnCl_2$ + 5 m NaCl solutions (see Fig. SI-15).

We turn briefly to the Monte Carlo (MC) simulation results in Figure 6a for the $ZnCl_2$ solution. In the dilute region, the onset of ion pairing is even more rapid than the CMD results while at higher concentrations there appears to be an incremental increase in the coordination just above 16 m Cl^- (8 m $ZnCl_2$). This apparent discontinuous nature of the Cl^- association is not unexpected for the coarse-grain lattice of MC that involves discrete ion-ion locations rather than a continuum of sites as in CMD. We recall that MC is expected to be a much more accurate representation of the equilibrium species at extreme concentrations since it provides a direct accounting for the strong, short-range inter-ionic interactions that are based upon realistic pair potentials while the CMD is an extrapolation of equilibrium constants derived from CMD 1D PMF calculations at 4.5 m $ZnCl_2$. In this regard, Figure 6a shows that the MC results are in somewhat better agreement with experiment than the CMD results at concentrations above 4.5 m $ZnCl_2$. MC also convincingly proves, in a way that is not possible via CMD, that the use of realistic ion-ion potentials yields at endpoint structure which saturates at $N_{Cl} = 2$. To some extent, the general agreement between MC and CMD at high concentrations, justifies the use of CMD as an approximation to this speciation. Finally, we note, for solutions with high Cl chloride concentrations in Figure 6b, the MC results are incomplete above 6 m C1- due to challenge of identifying coordination numbers on a lattice that are consistent with the continuum description.

Taken *en masse*, our combined experimental and theoretical results support several conclusions of strong contemporary interest. First, aqueous solutions of Zn halide salts show a quite rapid onset of ion pairing, and almost certainly exhibit a diverse population of partially chlorinated tetrahedral coordinations. Second, we have considerable evidence for the satisfying

result that $N_{Cl} \approx 2$ for concentrated pure solutions, i.e., that there is full anion coordination without polymerization. That being said, this inference is dependent on the assumption, made reasonable by the observed spectra but at least partially disputed by the classical molecular dynamics calculations, that solutions with lower Zn concentration and high anion activity fully reach $N_{Cl} = 4$, i.e., are dominated by $ZnCl_4^{2-}$ species. Finally, the hyper-local sensitivity of VTC-XES in solution, where second-shell coordination effects are yet even weaker than in a molecule or compound, is greatly beneficial for the study of ion pairing on an element-specific basis and should see broader future use.

IV. Conclusions

We report a combined experimental and theoretical treatment of ion pairing in Zn halide (ZnX_2, with X = Cl, Br) solutions over the full range of concentrations for pure solutions and over the full range of ion activities for 1 m solutions with added halide salts. Making particular use of the extreme local sensitivity of valence to core x-ray emission spectroscopy (VTC-XES) for this problem, we provide a new method to infer the average number of halide atoms coordinated to Zn^{+2}. This finds a strong onset to ion pairing and saturation at two halide atoms in the first shell for pure solutions but saturation at four halides, i.e., the ZnX_4^{2-} complex, for added salt solutions. Comparison to classical molecular dynamics finds generally good agreement with these results, with the exception of a strong prediction against the formation of ZnX_4^{2-}. This work informs ongoing discussion of the thermodynamics of Zn halide brines, of the physical chemistry of electrolytes for Zn halide batteries and suggests a broader use of VTC-XES for ion pairing studies and other problems involving metal complex formation in solution.

Acknowledgements

This work was supported by the Joint Center for Energy Storage Research, an Energy Innovation Hub funded by the U.S. Department of Energy. A.G.S. and N.R. were supported by the U.S. Department of Energy, Office of Science, Office of Basic Energy Sciences, Chemical Sciences, Geosciences, and Biosciences Division. This research used resources of the Advanced Photon Source, an Office of Science User Facility operated for the U.S. Department of Energy (DOE) Office of Science by Argonne National Laboratory and was supported by the U.S. DOE under contract no. DE-AC02-06CH11357. Work by N.G. was supported under project 72685, J.L.F. under project 16248, and G.K.S and C.J.M. under project 16249, funded by the U.S. Department of Energy (DOE), Office of Science, Office of Basic Energy Sciences, Division of Chemical Sciences, Geosciences, and Biosciences. This research benefited from computational resources provided by EMSL, a DOE Office of Science User Facility sponsored by the Office of Biological and Environmental Research and located at PNNL. PNNL is operated by Battelle Memorial Institute for the United States Department of Energy under DOE Contract No. DE-AC05-76RL1830. This research also used resources of the National Energy Research Scientific Computing Center (NERSC), a U.S. Department of Energy Office of Science User Facility operated under Contract No. DE-AC02-05CH11231.

References

1. Marcus Y, Hefter G. Ion pairing. Chemical Reviews. 2006;106(11):4585-621.
2. Castner EW, Wishart JF. Spotlight on ionic liquids. Journal of Chemical Physics. 2010;132(12):120901.
3. Wolynes PG. Dynamics of electrolyte-solutions. Annual Review of Physical Chemistry. 1980;31:345-76.
4. Endres F, El Abedin SZ. Air and water stable ionic liquids in physical chemistry. Physical Chemistry Chemical Physics. 2006;8(18):2101-16.
5. Hu YF, Peng XM. Effect of the Structures of Ionic Liquids on Their Physical Chemical Properties. Structures and Interactions of Ionic Liquids. 2014;151:141-74.
6. Kar M, Simons TJ, Forsyth M, MacFarlane DR. Ionic liquid electrolytes as a platform for rechargeable metal-air batteries: a perspective. Physical Chemistry Chemical Physics. 2014;16(35):18658-74.
7. Singh SK, Savoy AW. Ionic liquids synthesis and applications: An overview. Journal of Molecular Liquids. 2020;297:112038.
8. Liu W, Borg S, Etschmann B, Mei Y, Brugger J. An XAS study of speciation and thermodynamic properties of aqueous zinc bromide complexes at 25–150°C. Chemical Geology. 2012;298-299:57-69.
9. Mei Y, Sherman DM, Liu W, Etschmann B, Testemale D, Brugger J. Zinc complexation in chloride-rich hydrothermal fluids (25–600°C): A thermodynamic model derived from ab initio molecular dynamics. Geochimica et Cosmochimica Acta. 2015;150:265-84.
10. Demichelis R, Raiteri P, Gale JD, Quigley D, Gebauer D. Stable prenucleation mineral clusters are liquid-like ionic polymers. Nat Commun. 2011;2:590.
11. Dreier P, Rabe P. EXAFS-Study of the Zn2+ Coordination in Aqueous Halide Solutions. J Phys Colloques. 1986;47(C8):809-12.
12. Ji X. A perspective of ZnCl2 electrolytes: The physical and electrochemical properties. eScience. 2021;1:99-107.
13. Zhang C, Holoubek J, Wu XY, Daniyar A, Zhu LD, Chen C, et al. A ZnCl2 water-in-salt electrolyte for a reversible Zn metal anode. Chemical Communications. 2018;54(100):14097-9.
14. Zhang L, Rodriguez-Perez IA, Jiang H, Zhang C, Leonard DP, Guo QB, et al. ZnCl2 "Water-in-Salt" Electrolyte Transforms the Performance of Vanadium Oxide as a Zn Battery Cathode. Advanced Functional Materials. 2019;29(30):1902653.
15. Zhang C, Shin W, Zhu LD, Chen C, Neuefeind JC, Xu YK, et al. The electrolyte comprising more robust water and superhalides transforms Zn-metal anode reversibly and dendrite-free. Carbon Energy. 2021;3(2):339-48.
16. Wang F, Borodin O, Gao T, Fan X, Sun W, Han F, et al. Highly reversible zinc metal anode for aqueous batteries. Nature Materials. 2018;17(6):543-9.
17. Zhang H, Liu X, Qin B, Passerini S. Electrochemical intercalation of anions in graphite for high-voltage aqueous zinc battery. Journal of Power Sources. 2020;449:227594.
18. Rodríguez-Pérez IA, Zhang L, Wrogemann JM, Driscoll DM, Sushko ML, Han KS, et al. Enabling Natural Graphite in High-Voltage Aqueous Graphite || Zn Metal Dual-Ion Batteries. Advanced Energy Materials. 2020;10(41):2001256.

19. Song J, Xu K, Liu N, Reed D, Li X. Crossroads in the renaissance of rechargeable aqueous zinc batteries. Materials Today. 2021;45:191-212.
20. Zhang Y, Chen Z, Qiu H, Yang W, Zhao Z, Zhao J, et al. Pursuit of reversible Zn electrochemistry: a time-honored challenge towards low-cost and green energy storage. NPG Asia Materials. 2020;12(1):4.
21. Suo LM, Borodin O, Gao T, Olguin M, Ho J, Fan XL, et al. "Water-in-salt" electrolyte enables high-voltage aqueous lithium-ion chemistries. Science. 2015;350(6263):938-43.
22. Liu W, Etschmann B, Foran G, Shelley M, Brugger J. Deriving formation constants for aqueous metal complexes from XANES spectra: Zn2+ and Fe2+ chloride complexes in hypersaline solutions. American Mineralogist. 2007;92(5-6):761-70.
23. Ruaya JR, Seward TM. The stability of chlorozinc(II) complexes in hydrothermal solutions up to 350-degrees-C. Geochimica Et Cosmochimica Acta. 1986;50(5):651-61.
24. Gebauer D, Kellermeier M, Gale JD, Bergström L, Cölfen H. Pre-nucleation clusters as solute precursors in crystal- lisation. . Chem Soc Rev. 2014;43(7):2348 - 71.
25. Gebauer D, Raiteri P, Gale JD, Colfen H. On classical and non-classical views on nucleation. American Journal of Science. 2018;318(9):969-88.
26. Henzler K, Fetisov EO, Galib M, Baer MD, Legg BA, Borca C, et al. Supersaturated calcium carbonate solutions are classical. Sci Adv. 2018;4(1):eaao6283.
27. Larentzos JP, Criscenti LJ. A Molecular Dynamics Study of Alkaline Earth Metal-Chloride Complexation in Aqueous Solution. Journal of Physical Chemistry B. 2008;112(45):14243-50.
28. Wallace AF, Hedges LO, Fernandez-Martinez A, Raiteri P, Gale JD, Waychunas GA, et al. Microscopic Evidence for Liquid-Liquid Separation in Supersaturated CaCO3 Solutions. Science. 2013;341(6148):885-9.
29. Wang HW, Yuan K, Rampal N, Stack AG. Solution and Interface Structure and Dynamics in Geochemistry: Gateway to Link Elementary Processes to Mineral Nucleation and Growth. Crystal Growth & Design. 2022;22(1):853-70.
30. Rampal N, Wang HW, Biriukov D, Brady AB, Neuefeind JC, Predota M, et al. Local molecular environment drives speciation and reactivity of ion complexes in concentrated salt solution. Journal of Molecular Liquids. 2021;340:116898.
31. Wang HW, Graham TR, Mamontov E, Page K, Stack AG, Pearce CI. Countercations Control Local Specific Bonding Interactions and Nucleation Mechanisms in Concentrated Water-in-Salt Solutions. Journal of Physical Chemistry Letters. 2019;10(12):3318-25.
32. D'Angelo P, Zitolo A, Ceccacci F, Caminiti R, Aquilanti G. Structural characterization of zinc(II) chloride in aqueous solution and in the protic ionic liquid ethyl ammonium nitrate by x-ray absorption spectroscopy. The Journal of Chemical Physics. 2011;135(15):154509.
33. Kruh RF, Standley CL. An X-Ray Diffraction Study of Aqueous Zinc Chloride Solutions. Inorganic Chemistry. 1962;1(4):941-3.
34. Wilcox RJ, Losey BP, Folmer JCW, Martin JD, Zeller M, Sommer R. Crystalline and Liquid Structure of Zinc Chloride Trihydrate: A Unique Ionic Liquid. Inorganic Chemistry. 2015;54(3):1109-19.
35. Duboue-Dijon E, Mason PE, Fischer HE, Jungwirth P. Hydration and Ion Pairing in Aqueous Mg2+ and Zn2+ Solutions: Force-Field Description Aided by Neutron Scattering Experiments and Ab Initio Molecular Dynamics Simulations. Journal of Physical Chemistry B. 2018;122(13):3296-306.

36. Jahrman EP, Holden WM, Ditter AS, Mortensen DR, Seidler GT, Fister TT, et al. An improved laboratory-based x-ray absorption fine structure and x-ray emission spectrometer for analytical applications in materials chemistry research. Review of Scientific Instruments. 2019;90(2):024106.
37. Mortensen DR, Seidler GT, Kas JJ, Govind N, Schwartz CP, Pemmaraju S, et al. Benchmark results and theoretical treatments for valence-to-core x-ray emission spectroscopy in transition metal compounds. Physical Review B. 2017;96(12):125136.
38. Bearden JA. X-ray Wavelengths. Reviews of Modern Physics. 1967;39(1):78.
39. Kraft S, Stümpel J, Becker P, Kuetgens U. High resolution x-ray absorption spectroscopy with absolute energy calibration for the determination of absorption edge energies. Review of Scientific Instruments. 1996;67(3):681-7.
40. Ravel B, Newville M. ATHENA, ARTEMIS, HEPHAESTUS: data analysis for X-ray absorption spectroscopy using IFEFFIT. Journal of Synchrotron Radiation. 2005;12(4):537-41.
41. Apra E, Bylaska EJ, de Jong WA, Govind N, Kowalski K, Straatsma TP, et al. NWChem: Past, present, and future. Journal of Chemical Physics. 2020;152(18):184102.
42. Valiev M, Bylaska EJ, Govind N, Kowalski K, Straatsma TP, Van Dam HJJ, et al. NWChem: A comprehensive and scalable open-source solution for large scale molecular simulations. Computer Physics Communications. 2010;181(9):1477-89.
43. Dolg M, Wedig U, Stoll H, Preuss H. Energy-adjusted ab-initio pseudopotentials for the 1st-row transition-elements. Journal of Chemical Physics. 1987;86(2):866-72.
44. Bergner A, Dolg M, Kuchle W, Stoll H, Preuss H. Ab-initio energy-adjusted pseodopotentials for elements of groups 13-17. Molecular Physics. 1993;80(6):1431-41.
45. Pritchard BP, Altarawy D, Didier B, Gibson TD, Windus TL. New Basis Set Exchange: An Open, Up-to-Date Resource for the Molecular Sciences Community. Journal of Chemical Information and Modeling. 2019;59(11):4814-20.
46. Perdew JP, Ernzerhof M, Burke K. Rationale for mixing exact exchange with density functional approximations. The Journal of Chemical Physics. 1996;105(22):9982-5.
47. Klamt A, Schuurmann G. COSMO - A new approach to dielectric screening in solvents with explicit expressions for the screening energy and its gradient. Journal of the Chemical Society-Perkin Transactions 2. 1993(5):799-805.
48. Lopata K, Van Kuiken BE, Khalil M, Govind N. Linear-Response and Real-Time Time-Dependent Density Functional Theory Studies of Core-Level Near-Edge X-Ray Absorption. Journal of Chemical Theory and Computation. 2012;8(9):3284-92.
49. Zhang Y, Mukamel S, Khalil M, Govind N. Simulating Valence-to-Core X-ray Emission Spectroscopy of Transition Metal Complexes with Time-Dependent Density Functional Theory. Journal of Chemical Theory and Computation. 2015;11(12):5804-9.
50. Noro T, Sekiya M, Koga T. Segmented contracted basis sets for atoms H through Xe: Sapporo-(DK)-nZP sets (n = D, T, Q). Theoretical Chemistry Accounts. 2012;131:1124.
51. Plimpton S. Fast parallel algorithms for short-range molecular-dynamics. Journal of Computational Physics. 1995;117(1):1-19.
52. Berendsen HJC, Grigera JR, Straatsma TP. The missing term in effective pair potentials. Journal of Physical Chemistry. 1987;91(24):6269-71.

53. Pluharova E, Mason PE, Jungwirth P. Ion Pairing in Aqueous Lithium Salt Solutions with Monovalent and Divalent Counter-Anions. Journal of Physical Chemistry A. 2013;117(46):11766-73.
54. Nguyen MTH, Tichacek O, Martinez-Seara H, Mason PE, Jungwirth P. Resolving the Equal Number Density Puzzle: Molecular Picture from Simulations of LiCl(aq) and NaCl(aq). Journal of Physical Chemistry B. 2021;125(12):3153-62.
55. Brown WM, Kohlmeyer A, Plimpton SJ, Tharrington AN. Implementing molecular dynamics on hybrid high performance computers - Particle-particle particle-mesh. Computer Physics Communications. 2012;183(3):449-59.
56. Martinez L, Andrade R, Birgin EG, Martinez JM. PACKMOL: A Package for Building Initial Configurations for Molecular Dynamics Simulations. Journal of Computational Chemistry. 2009;30(13):2157-64.
57. Parkhurst DL, Appelo CAJ. User's Guide to PHREEQC (Version 2): A Computer Program for Speciation, Batch-Reaction, One-Dimensional Transport, and Inverse Geochemical Calculations.; 1999.
58. Davies CW. Ion Association. London: Butterworths. 1962:37-53.
59. Drever JI. The Geochemistry of Natural Waters: Surface and Groundwater Environments. Upper Saddle River, New Jersey: Prentice-Hall Inc.; 1997.
60. Ewald PP. Die Berechnung optischer und elektrostatischer Gitterpotentiale. Annalen der Physik. 1921;369(3):253-87.
61. Frenkel D, Smit B. Understanding Molecular Simulation: From Algorithms to Applications. 2 ed: Academic Press; 2001.
62. Chen YS, Fulton JL, Partenheimer W. A XANES and EXAFS study of hydration and ion pairing in ambient aqueous MnBr2 solutions. Journal of Solution Chemistry. 2005;34(9):993-1007.
63. Fulton JL, Heald SM, Badyal YS, Simonson JM. Understanding the effects of concentration on the solvation structure of Ca2+ in aqueous solution. I: The perspective on local structure from EXAFS and XANES. Journal of Physical Chemistry A. 2003;107(23):4688-96.
64. Hoffmann MM, Darab JG, Palmer BJ, Fulton JL. A transition in the Ni2+ complex structure from six- to four-coordinate upon formation of ion pair species in supercritical water: An X-ray absorption fine structure, near-infrared, and molecular dynamics study. Journal of Physical Chemistry A. 1999;103(42):8471-82.
65. Gallo E, Bonino F, Swarbrick JC, Petrenko T, Piovano A, Bordiga S, et al. Preference towards Five-Coordination in Ti Silicalite-1 upon Molecular Adsorption. Chemphyschem. 2013;14(1):79-83.
66. Hennings E, Schmidt H, Voigt W. Crystal structures of ZnCl2.2.5H2O, ZnCl2.3H2O and ZnCl2.4.5H2O. Acta Crystallographica Section E. 2014;70(12):515-8.
67. Maeda M, Ito T, Hori M, Johansson G. The structure of zinc chloride complexes in aqueous solution. Zeitschrift Fur Naturforschung Section a-a Journal of Physical Sciences. 1996;51(1-2):63-70.
68. Biriukov D, Wang HW, Rampal N, Tempra C, Kula P, Neuefeind JC, et al. The "good," the "bad," and the "hidden" in neutron scattering and molecular dynamics of ionic aqueous solutions. Journal of Chemical Physics. 2022;156(19):194505.

69. Anovitz LM, Huestis P, Rampal N, Stack AG, LaVerne JA, Zhang X, et al. Frustrated Coulombic and Cation Size Effects on Nanoscale Boehmite Aggregation: A Tumbler Small- and Ultra-Small-Angle Neutron Scattering Study. Journal of Physical Chemistry C. 2022;126(9):4391-414.